

Exploiting Low Rank Covariance Structures for Computing High-Dimensional Normal and Student- t Probabilities

Jian Cao ¹, Marc G. Genton ¹, David E. Keyes ¹, and George M. Turkiyyah ²

December 23, 2020

Abstract

We present a preconditioned Monte Carlo method for computing high-dimensional multivariate normal and Student- t probabilities arising in spatial statistics. The approach combines a tile-low-rank representation of covariance matrices with a block-reordering scheme for efficient Quasi-Monte Carlo simulation. The tile-low-rank representation decomposes the high-dimensional problem into many diagonal-block-size problems and low-rank connections. The block-reordering scheme reorders between and within the diagonal blocks to reduce the impact of integration variables from right to left, thus improving the Monte Carlo convergence rate. Simulations up to dimension 65,536 suggest that the new method can improve the run time by an order of magnitude compared with the non-reordered tile-low-rank Quasi-Monte Carlo method and two orders of magnitude compared with the dense Quasi-Monte Carlo method. Our method also forms a strong substitute for the approximate conditioning methods as a more robust estimation with error guarantees. An application study to wind stochastic generators is provided to illustrate that the new computational method makes the maximum likelihood estimation feasible for high-dimensional skew-normal random fields.

Keywords: Adaptive cross approximation, Block reordering, Hierarchical matrix, Skew-normal random field, Tile-low-rank matrix.

¹ CEMSE Division, Extreme Computing Research Center, King Abdullah University of Science and Technology, Thuwal 23955-6900, Saudi Arabia.

E-mail: {jian.cao, marc.genton, david.keyes}@kaust.edu.sa

This research was supported by King Abdullah University of Science and Technology (KAUST).

² Department of Computer Science, American University of Beirut, Beirut, Lebanon.

E-mail: gt02@aub.edu.lb

1 Introduction

The multivariate normal (MVN) probability appears frequently in statistical applications. For example, the probability density functions of several skew-normal (Genton, 2004; Azzalini and Capitanio, 2014; Arellano-Valle et al., 2006) and Bayesian probit (Durante, 2019) models involve MVN cumulative distribution functions. It is also needed in computing the excursion and contour regions discussed in Bolin and Lindgren (2015). For many of these applications, the MVN probability is treated as a bottleneck and approximating the covariance matrix is often applied in high dimensions. The MVN probability is one example of numerical integration, where the quadrature-based methods are typically not applicable in hundreds of dimensions. The Monte-Carlo-based methods are more flexible but their convergence rate is subject to several factors. In this paper, we aim to reduce the time costs and extend the limits for computing MVN probabilities.

The prevalent algorithm for computing MVN probabilities is based on the separation-of-variable (SOV) technique (Genz, 1992), which converts the integration region to the unit hypercube to improve the convergence rate. This method is likely more robust than its improved variants but has poor scalability, with the costs of $O(n^3)$ for the Cholesky factorization and $O(n^2)$ per MC sample, where n is the MVN problem dimension. The state-of-the-art methods for computing the MVN probability include the hierarchical Quasi-Monte Carlo (QMC) method (Genton et al., 2018), the minimax tilting method (Botev, 2017), and the hierarchical conditioning method (Cao et al., 2019). The hierarchical QMC method reduced the costs per sample through the hierarchical representation (Hackbusch, 2015) of the Cholesky factor. Its drawback is its incompatibility with variable reordering and hence, its inability to benefit from an improved convergence rate. The minimax tilting method significantly improved the convergence rate with a well-designed proposal density but it needed to solve a non-linear optimization problem with $2n$ parameters to identify the proposal distribution. The hierarchical conditioning method pursued minimum time costs by updating integration limits with truncated expectations. However, it

lacks an error estimation and is less accurate than its competitors.

This paper builds on the original SOV method in Genz (1992) and introduces a variant that has better performance than the hierarchical QMC method in Genton et al. (2018). Specifically, we combine the SOV method with the tile-low-rank (TLR) representation (Akbulak et al., 2017), which improves efficiency from three aspects. First, the overall low-rank feature becomes stronger under the TLR representation, for which the Cholesky factorization can be based on fast truncation algorithms. Secondly, the TLR representation is compatible with block-wise variable reordering and hence, benefits from a higher convergence rate. Lastly, the storage costs of the TLR representation can be even smaller than those of the hierarchical representation, which indicates even lower costs per MC sample. In this paper, we do not resort to the importance sampling technique because the costs for finding the optimal proposal density described in Botev (2017) make the algorithm difficult to scale beyond 2,000 dimensions. Instead, we show that the estimations are still reliable in terms of log-probabilities without importance sampling. As for variable reordering, we propose an iterative version of the original block reordering in Cao et al. (2019) that further improves the convergence rate and performs the Cholesky factorization simultaneously. The corresponding algorithm for multivariate Student- t (MVT) probabilities is also developed. Finally, we demonstrate the capability of our methods in tens of thousands of dimensions with two maximum likelihood estimation (MLE) studies based on simulated data and a wind dataset.

The remainder of this paper is structured as follows. In Section 2, we introduce the SOV technique (Genz and Bretz, 2009) for MVN and MVT problems and describe dense QMC algorithms for both probabilities. In Section 3, we demonstrate the incompatibility between the hierarchical structure and the block reordering, which leads to the choice of the TLR structure. An improved version of the block reordering from Cao et al. (2019) is proposed. In Section 4, we compare the dense QMC method, the TLR QMC method, and the preconditioned TLR QMC methods with a focus on high-dimensional MVN and MVT probabilities. In Section 5, we es-

timate the parameters for simulated high-dimensional skew-normal random fields as well as fit the skew-normal model to a large wind speed dataset of Saudi Arabia as examples where the methods developed in this paper can be applied. Section 6 concludes the paper.

2 SOV for MVN and MVT Probabilities

The SOV technique transforms the integration region into the unit hypercube, where efficient QMC rules can improve the convergence rate. The SOV of MVN probabilities is based on the Cholesky factor of the covariance matrix (Genz, 1992) and this naturally leads to the second form of SOV for MVT probabilities (Genz and Bretz, 2002). The two forms of SOV for MVT probabilities have been derived in Genz (1992) and Genz and Bretz (2002). In this paper, we summarize the derivations for completeness.

2.1 SOV for MVN integrations

We denote an n -dimensional MVN probability with $\Phi_n(\mathbf{a}, \mathbf{b}; \boldsymbol{\mu}, \boldsymbol{\Sigma})$, where (\mathbf{a}, \mathbf{b}) defines a hyperrectangle-shaped integration region, $\boldsymbol{\mu}$ is the mean vector, and $\boldsymbol{\Sigma}$ is the covariance matrix. The MVN probability has the form:

$$\Phi_n(\mathbf{a}, \mathbf{b}; \boldsymbol{\mu}, \boldsymbol{\Sigma}) = \int_{\mathbf{a}-\boldsymbol{\mu}}^{\mathbf{b}-\boldsymbol{\mu}} \frac{1}{\sqrt{(2\pi)^n |\boldsymbol{\Sigma}|}} \exp\left(-\frac{1}{2} \mathbf{x}^\top \boldsymbol{\Sigma}^{-1} \mathbf{x}\right) d\mathbf{x}. \quad (1)$$

Without loss of generality, we set $\boldsymbol{\mu} = \mathbf{0}$ and denote the n -dimensional MVN probability with $\Phi_n(\mathbf{a}, \mathbf{b}; \boldsymbol{\Sigma})$. We use \mathbf{C} to represent the lower Cholesky factor of $\boldsymbol{\Sigma} = \mathbf{C}\mathbf{C}^\top$ and c_{ij} to represent the element on the i -th row and j -th column of \mathbf{C} . Following the procedure in Genz (1992), we can transform $\Phi_n(\mathbf{a}, \mathbf{b}; \boldsymbol{\Sigma})$ into:

$$\Phi_n(\mathbf{a}, \mathbf{b}; \boldsymbol{\Sigma}) = (e_1 - d_1) \int_0^1 (e_2 - d_2) \cdots \int_0^1 (e_n - d_n) \int_0^1 d\mathbf{w}, \quad (2)$$

where $d_i = \Phi\{(a_i - \sum_{j=1}^{i-1} c_{ij}y_j)/c_{ii}\}$, $e_i = \Phi\{(b_i - \sum_{j=1}^{i-1} c_{ij}y_j)/c_{ii}\}$, $y_j = \Phi^{-1}\{d_j + w_j(e_j - d_j)\}$, and $\Phi(\cdot)$ is the cumulative distribution function (cdf) of the standard normal distribution.

The integration region is transformed into $[0, 1]^n$ and efficient sampling rules can be applied to simulate \mathbf{w} , although the integrand is difficult to compute in parallel because d_i and e_i depend on $\{y_j, j = 1, \dots, i-1\}$ while y_i depends on d_i and e_i . Only univariate standard normal probabilities and quantile functions are needed, which can be readily obtained with the high efficiency of scientific computing libraries, for example, the Intel MKL. The Cholesky factorization has a complexity of $O(n^3)$ but modern CPUs and libraries have been developed to handle matrices with more than 10,000 dimensions with ease.

We use ‘mvn’ to denote the integrand function of Equation (2), whose pseudocode was originally proposed in Genz (1992). Because the ‘mvn’ function is also the subroutine in other functions of this paper, we summarize it here in Algorithm 2.1a. The algorithm returns P , the probability estimate from one sample and \mathbf{y} whose coefficients are described in Equation (2). Keeping \mathbf{a} , \mathbf{b} , and \mathbf{C} unchanged, the mean and standard deviation of the outputs P from a

Algorithm 2.1a QMC for MVN probabilities

```

1: mvn( $\mathbf{C}$ ,  $\mathbf{a}$ ,  $\mathbf{b}$ ,  $\mathbf{w}$ )
2:  $n \leftarrow \dim(\mathbf{C})$ ,  $s \leftarrow 0$ ,  $\mathbf{y} \leftarrow \mathbf{0}$ , and  $P \leftarrow 1$ 
3: for  $i = 1 : n$  do
4:   if  $i > 1$  then
5:      $s \leftarrow \mathbf{C}(i, 1 : i - 1)\mathbf{y}(1 : i - 1)$ 
6:   end if
7:    $a' \leftarrow \frac{a_i - s}{C_{i,i}}$ , and  $b' \leftarrow \frac{b_i - s}{C_{i,i}}$ 
8:    $y_i \leftarrow \Phi^{-1}[w_i\{\Phi(b') - \Phi(a')\}]$ 
9:    $P \leftarrow P \cdot \{\Phi(b') - \Phi(a')\}$ 
10: end for
11: return  $P$  and  $\mathbf{y}$ 

```

set of well designed \mathbf{w} , usually conforming to a Quasi-Monte Carlo rule, form the probability and error estimates. In our implementation, we employ the Richtmyer Quasi-Monte Carlo rule (Richtmyer, 1951), where the batch number is usually much smaller than the batch size.

2.2 SOV for MVT integrations

We denote an n -dimensional MVT probability with $T_n(\mathbf{a}, \mathbf{b}; \boldsymbol{\mu}, \boldsymbol{\Sigma}, \nu)$, where ν is the degrees of freedom. Here, $\boldsymbol{\mu}$ is the mean vector and $\boldsymbol{\Sigma}$ is the scale matrix. To simplify the notations, $\boldsymbol{\mu}$ is again assumed to be $\mathbf{0}$. There are two common equivalent definitions for T_n , of which the first one is:

$$T_n(\mathbf{a}, \mathbf{b}; \boldsymbol{\Sigma}, \nu) = \frac{\Gamma(\frac{\nu+n}{2})}{\Gamma(\frac{\nu}{2})\sqrt{|\boldsymbol{\Sigma}|}(\nu\pi)^n} \int_{a_1}^{b_1} \cdots \int_{a_n}^{b_n} \left(1 + \frac{\mathbf{x}^\top \boldsymbol{\Sigma}^{-1} \mathbf{x}}{\nu}\right)^{-\frac{\nu+n}{2}} d\mathbf{x}, \quad (3)$$

where $\Gamma(\cdot)$ is the gamma function. Based on this definition, Genz and Bretz (1999) transformed the integration into the n -dimensional hypercube, where the inner integration limits depend on the outer integration variables. However, the integration needs to compute the cdf and the quantile function of the univariate Student- t distribution at each integration variable. A second equivalent form defines T_n as a scale mixture of the MVN probability, specifically:

$$T_n(\mathbf{a}, \mathbf{b}; \boldsymbol{\Sigma}, \nu) = \frac{2^{1-\frac{\nu}{2}}}{\Gamma(\frac{\nu}{2})} \int_0^\infty s^{\nu-1} e^{-s^2/2} \Phi_n\left(\frac{s\mathbf{a}}{\sqrt{\nu}}, \frac{s\mathbf{b}}{\sqrt{\nu}}; \boldsymbol{\Sigma}\right) ds, \quad (4a)$$

$$= E\left[\Phi_n\left(\frac{S\mathbf{a}}{\sqrt{\nu}}, \frac{S\mathbf{b}}{\sqrt{\nu}}; \boldsymbol{\Sigma}\right)\right]. \quad (4b)$$

The density of a χ -distribution random variable, S , with degrees of freedom ν , is exactly $\frac{2^{1-\frac{\nu}{2}}}{\Gamma(\frac{\nu}{2})} s^{\nu-1} e^{-s^2/2}$, $s > 0$. Thus, $T_n(\mathbf{a}, \mathbf{b}; \boldsymbol{\Sigma}, \nu)$ can be also written as Equation (4b). The integrand boils down to the MVN probability discussed in the previous section. Hence, we can apply a Quasi-Monte Carlo rule in the $(n+1)$ -dimensional hypercube to approximate this expectation, where only the cdf and the quantile function of the univariate standard normal distribution are involved. It is worth pointing out that considering T_n as a one-dimensional integration of Φ_n and applying quadrature is much more expensive than integrating directly in $(n+1)$ dimensions.

We describe the integrand functions based on the two SOV schemes in Algorithm 2.2a and Algorithm 2.2b, corresponding to Equation (3) and Equation (4a), respectively. Algorithm 2.2a calls the univariate Student- t cdf and the quantile function with an increasing value of degrees of freedom at each iteration whereas Algorithm 2.2b relies on (w_0, \mathbf{w}) from an $(n+1)$ -dimensional

Algorithm 2.2a QMC for MVT probabilities based on Equation (3)

```

1: mvt(C, a, b,  $\nu$ , w)
2:  $n \leftarrow \dim(\mathbf{C})$ ,  $s \leftarrow 0$ ,  $ssq \leftarrow 0$ ,  $\mathbf{y} \leftarrow \mathbf{0}$ , and  $P \leftarrow 1$ 
3: for  $i = 1 : n$  do
4:   if  $i > 1$  then
5:      $s \leftarrow \mathbf{C}(i, 1 : i - 1)\mathbf{y}(1 : i - 1)$ 
6:   end if
7:    $a' \leftarrow \frac{a_i - s}{\mathbf{C}_{i,i} \cdot \sqrt{\nu + ssq} \cdot (\nu + i)}$  and  $b' \leftarrow \frac{b_i - s}{\mathbf{C}_{i,i} \cdot \sqrt{\nu + ssq} \cdot (\nu + i)}$ 
8:    $y_i \leftarrow T_{\nu+i}^{-1} [w_i \{T_{\nu+i}(b') - T_{\nu+i}(a')\} + T_{\nu+i}(a')] \cdot \sqrt{\frac{\nu + ssq}{\nu + i}}$ 
9:    $P \leftarrow P \cdot \{T_{\nu+i}(b') - T_{\nu+i}(a')\}$ 
10:   $ssq \leftarrow ssq + y_i^2$ 
11: end for
12: return  $P$ 

```

Table 1: Relative error and time of the three algorithms. ‘mvt 1’, ‘mvt 2’, and ‘mvn’ refer to Algorithm 2.2a, Algorithm 2.2b, and Algorithm 2.1a. The covariance matrix is generated from a 2D exponential model, $\exp(-\|\mathbf{h}\|/\beta)$, where $\beta = 0.1$, based on n random points in the unit square. The lower integration limits are fixed at $-\infty$ and the upper limits are generated from $N(5.5, 1.25^2)$. ν is set as 10 for the ‘mvt’ algorithms. The upper row is the average relative estimation error and the lower row is the average computation time over 20 iterations. All three algorithms have the same sample size of $N = 10^4$.

n	16	64	256	1,024	4,096
mvt 1	0.0% <i>0.7s</i>	0.2% <i>3.0s</i>	0.7% <i>13.3s</i>	1.4% <i>58.7s</i>	4.2% <i>283.1s</i>
mvt 2	0.0% <i>0.0s</i>	0.0% <i>0.0s</i>	0.2% <i>0.2s</i>	0.4% <i>2.0s</i>	1.3% <i>40.8s</i>
mvn	0.0% <i>0.0s</i>	0.0% <i>0.0s</i>	0.1% <i>0.2s</i>	0.4% <i>2.0s</i>	1.2% <i>40.1s</i>

Quasi-Monte Carlo rule and calls the ‘mvn’ kernel from Algorithm 2.1a with the scaled integration limits. We use single-quoted ‘mvn’ and ‘mvt’ to denote the corresponding algorithms to distinguish them from the uppercase MVN and MVT used for multivariate normal and Student- t in this paper.

A numerical comparison between Algorithm 2.2a and Algorithm 2.2b is shown in Table 1.

Algorithm 2.2b QMC for MVT probabilities based on Equation (4a)

```

1: mvt(C, a, b,  $\nu$ ,  $w_0$ , w)
2:  $\mathbf{a}' \leftarrow \frac{\chi_{\nu}^{-1}(w_0)}{\sqrt{\nu}}\mathbf{a}$ ,  $\mathbf{b}' \leftarrow \frac{\chi_{\nu}^{-1}(w_0)}{\sqrt{\nu}}\mathbf{b}$ 
3: return mvn(C,  $\mathbf{a}'$ ,  $\mathbf{b}'$ , w)

```

The counterpart for MVN probabilities (Algorithm 2.1a) is included as a benchmark. The table indicates that the first definition as in Equation (3) leads to an implementation slower by one order of magnitude. Additionally, the convergence rate from Equation (3) is also worse than that from Equation (4a). Although the univariate Student- t cdf and quantile function are computed the same number of times as their standard normal counterparts, their computation takes much more time and probably produces lower accuracy due to the lack of optimized libraries. Due to its performance advantage, we refer to Algorithm 2.2b as the ‘mvt’ algorithm from this point on. It has negligible marginal complexity over the ‘mvn’ algorithm since the only additional step is scaling the integration limits.

3 Low-rank Representation and Reordering for MVN and MVT Probabilities

3.1 Overview

More flexible than quadrature methods, Monte Carlo (MC) procedures provide several viable options for computing MVN and MVT probabilities. The cost of these computations depends on the product of the number of MC samples, N , needed to achieve a desired accuracy and the cost per MC sample. Under the standard dense representation of covariance, the computational complexity for each sample is $O(n^2)$ as shown in Algorithm 2.1a and Algorithm 2.2b. Genton et al. (2018) proposed using the hierarchical representation for the Cholesky factor, illustrated in Figure 1, which reduced the complexity per sample to $O(kn \log n)$, where k is a nominal local rank of the matrix blocks. Using nested bases in the hierarchical representation (Boukaram et al., 2019), it is possible to reduce this cost further to an asymptotically optimal $O(kn)$.

Small local ranks k in the hierarchical representation depend on the separability of the underlying geometry and are directly affected by the ordering of the underlying point set. When the row cluster and the column cluster of an off-diagonal matrix block are well separated spatially,

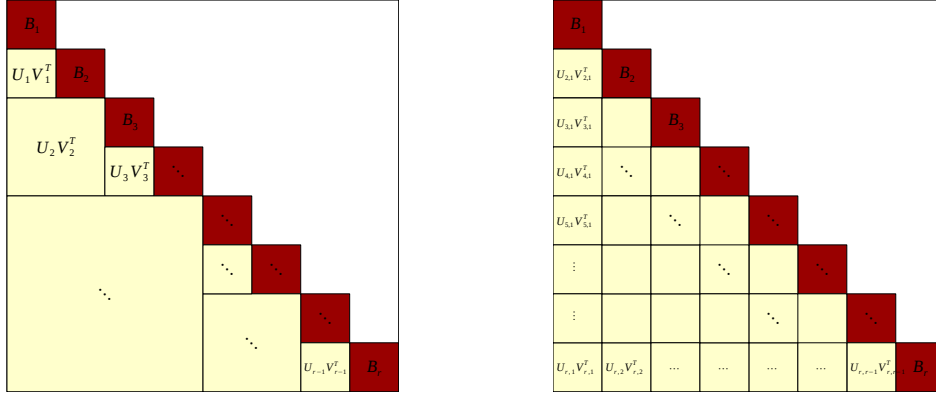


Figure 1: Structures of hierarchical (left) and tile-low-rank (right) matrices.

the ranks of these blocks tend to be rather small, growing very weakly with the problem dimension n . When the geometry is a subset of \mathbb{R}^2 or \mathbb{R}^3 , a space-filling curve, or a spatial partitioning method in combination with a space-filling curve, may be used for indexing to keep the index distances reasonably consistent with the spatial distances. The point set is then further divided into blocks (clusters) according to these indices to build the hierarchical representation.

The optimal ordering for reducing the cost per Monte Carlo sample however is unfortunately generally not the optimal ordering for reducing the total number of samples N . A proper reordering scheme that takes into account the widths of the integration limits of the MVN and MVT probabilities can have a substantial effect on reducing the variance of the estimates, making the numerical methods far more effective relative to a default ordering (Schervish, 1984; Genz and Bretz, 2009). Trinh and Genz (2015) analyzed ordering heuristics and found that a univariate reordering scheme, that sorts the variables so that the outermost integration variables have the smallest expected values, significantly increased the estimation accuracy. This heuristic was more effective overall than more expensive bivariate reordering schemes that might further reduce the number of samples needed. In Cao et al. (2019), a block reordering scheme was proposed with the hierarchical matrix representations used in high dimensions. Specifically, within each diagonal block \mathbf{B}_i , univariate reordering was applied and the blocks were reordered based on their estimated probabilities using this univariate reordering scheme.

The important point here is that these reordering schemes shuffle the variables based on their integration limits to achieve better convergence for the integration, measured by the number of samples needed. They produce different orders from the geometry-oriented ordering obtained by spatial partitioning methods or space-filling curves. The reordering increases the local ranks k of the hierarchical representation making the per-sample computation more expensive.

In this paper, we seek a better middle ground between the geometry-oriented and the integration-oriented orderings by combining a block reordering scheme with the tile-low-rank representation of covariance illustrated in Figure 1. We also introduce the TLR versions of the QMC algorithms for computing MVN and MVT probabilities.

3.2 TLR as a practical representation for MVN and MVT

To show the rank increase under the hierarchical representation due to integration-oriented orderings, we consider an MVN problem, where the integration limits are randomly generated and independent from the geometry. We use Morton order (Samet, 1990) as a geometry-oriented ordering to compare with the integration-oriented block ordering scheme proposed in Cao et al. (2019) with respect to constructing the hierarchical Cholesky factor. Figure 2 highlights the sharp increase in local ranks, represented by the storage costs when Morton order is substituted with the block reordering. The initial covariance matrices are built with the 2D exponential covariance model, $\exp(-\|\mathbf{h}\|/\beta)$, $\beta = 0.3$, based on a perturbed grid in the unit square as described in Section 5.2. Similar to Genton et al. (2018) and Cao et al. (2019), the hierarchical matrix is built under the weak admissible condition and the rank of each block is defined as the number of singular values above an absolute threshold of 10^{-2} .

Every off-diagonal block touching the main diagonal is represented as $\mathbf{U}\mathbf{V}^\top$, where \mathbf{U} and \mathbf{V} are thin matrices. This representation is beneficial only if the ranks of the off-diagonal blocks are small, which typically originates from well-defined separability (Hackbusch, 2015). However, the two sets of spatial locations corresponding to the rows and columns of large off-diagonal

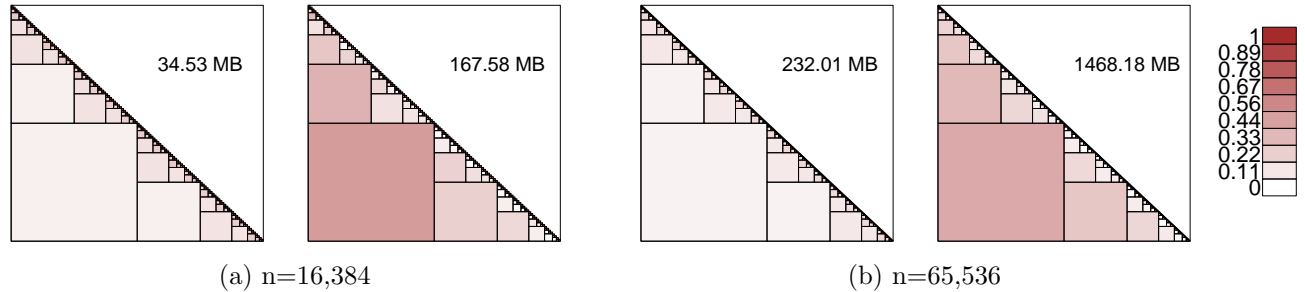


Figure 2: Increase in local rank and memory footprint of the Cholesky factor of a hierarchical matrix due to integration-oriented ordering. In each subfigure, the left panel is under Morton order while the right panel is under the block reordering. The diagonal block size is \sqrt{n} . The storage cost for the lower triangular part of the Cholesky factor is marked in each subfigure. The color for each block is coded by the logarithm of the rank-to-block-size ratio, linearly transformed into $(0, 1)$.

blocks become less separable under the block reordering compared with Morton order because the former is equivalent to block shuffling when each block’s integration limits are independent and identically distributed. The changes in the storage cost and the rank-to-block-size ratio in Figure 2 is a numerical proof of the incompatibility between the hierarchical structure and the integration-oriented orderings.

We now consider the rank impact on the TLR structure from the same change in the ordering scheme. Figure 3 shows that the average rank of the off-diagonal blocks in the TLR structure

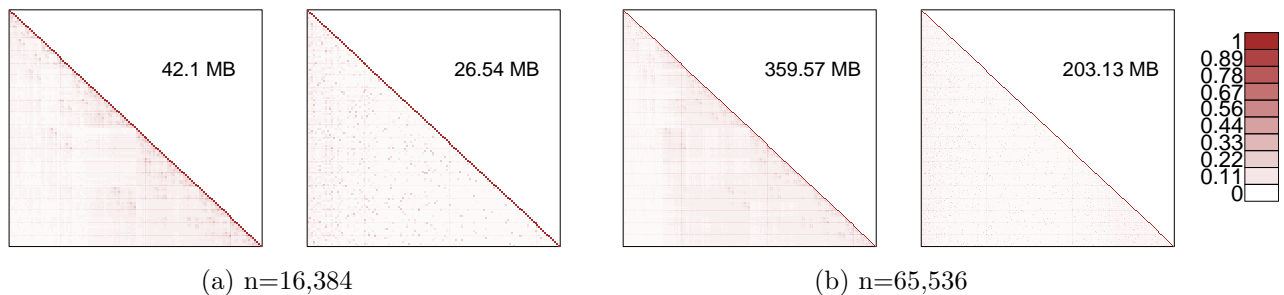


Figure 3: Change in local rank and memory footprint of the Cholesky factor of TLR matrix due to integration-oriented ordering. In each subfigure, the left panel is under Morton order while the right panel is under the block reordering. The diagonal block size is \sqrt{n} . The storage cost for the lower triangular part of the Cholesky factor is marked in each subfigure. The color for each block is coded by the logarithm of the rank-to-block-size ratio, linearly transformed into $(0, 1)$.

even decreases when applying the block reordering scheme, which shuffles the diagonal blocks.

This numerical result may appear odd but an explanation is given from two perspectives.

Firstly, the collection of local ranks in the TLR covariance matrix does not change. The block reordering changes the order of blocks but does not switch variables from different blocks and hence, the new TLR covariance matrix merely rearranges the previous off-diagonal blocks. Secondly, the magnitude of the Schur complement decreases faster along with the block column index under the block reordering. Intuitively, the Schur complement at block column i , $\Sigma_{i:r,i:r} - \Sigma_{i:r,1:i-1}\Sigma_{1:i-1,1:i-1}^{-1}\Sigma_{i:r,1:i-1}^\top$, is the conditional covariance matrix for blocks i to r given blocks 1 to $i - 1$. We argue that for most spatial correlation matrices, the Schur complement given a clustered set of spatial locations is bigger in magnitude than that given a set of scattered locations of the same size. This is treated as a heuristic without proof since it is not the focus of the paper. One measure for magnitude is the Frobenius norm. The Frobenius norm of a Cholesky factor is equal to the square root of the trace of the corresponding covariance matrix. Since $\mathbf{C}_{i:r,i:r}$ is the Cholesky factor of the corresponding Schur complement, the magnitude of the Cholesky factor also decreases faster along with the block column index under the block reordering. Overall, these two aspects lead to a smaller average local rank for the block reordering. It is worth noting that the absolute truncation usually demonstrates better efficiency than the relative one for correlation matrices because all coefficients belong to $[-1, 1]$ and the magnitude ratio between different blocks varies significantly.

We conclude that the TLR structure is compatible and even creates a synergy with the block reordering. There are also two practical benefits compared with the hierarchical structure with the weak admissibility. First, fast approximation algorithms, for example, the adaptive cross approximation (ACA) (Bebendorf, 2011), can be more reliably applied under TLR due to its lower ranks. Second, the regularity of the flat structure of TLR benefits more directly from modern hardware architectures. The reordering for MVT problems shares the same principle. Specifically, because the expectation of S from Equation (4a) is $\sqrt{2}\Gamma\{(\nu + 1)/2\}/\Gamma(\nu/2)$, converging to $\sqrt{\nu}$ quickly as ν increases, Genz and Bretz (2002) proposed substituting S with $\sqrt{\nu}$ and the reordering

becomes exactly the same as that for the MVN probability.

3.3 Reordering schemes and TLR factorizations

The block reordering scheme was proposed in Cao et al. (2019) and shown to improve the estimation accuracy of the conditioning method at a lower cost than the univariate or bivariate reordering scheme introduced in Trinh and Genz (2015). In this paper, we improve the original block reordering scheme by ordering the blocks of variables iteratively. The new iterative block reordering, similar to the block version of the univariate reordering scheme in Trinh and Genz (2015), enjoys a higher convergence rate and produces the Cholesky factor simultaneously.

Algorithm 3.3a describes the original block reordering scheme proposed in Cao et al. (2019) while Algorithm 3.3b is the iterative version that produces the Cholesky factor. We use $\Sigma_{i,j}$ to represent the (i, j) -th size- m block of Σ . Similar notations are also used for \mathbf{a} and \mathbf{b} . The symbol \rightleftharpoons indicates the switching of coefficients, rows, or columns. Variables can be overwritten by themselves after computations for computational benefits. When $i \neq j$, $\Sigma_{i,j}$ is stored in the low-rank format. The blue lines in Algorithm 3.3b mark the matrix operations that are also in the TLR Cholesky factorization (Akbudak et al., 2017). If we ignore the cost for steps 5 and 9, the complexity of Algorithm 3.3b is the same as the TLR Cholesky factorization. Although the complexity for accurately computing Φ_m and the truncated expectations is high, the univariate conditioning method (Trinh and Genz, 2015), with a complexity of $O(m^3)$, can provide an estimate for both that is indicative enough. Algorithm 3.3a ignores the correlation between the m -dimensional blocks and also uses the univariate conditioning method for approximating Φ_m . Therefore, the block reordering scheme has a total complexity of $O(nm^2)$ but requires a succeeding Cholesky factorization while the block reordering has additional complexity of $O(n^2m)$ over the TLR Cholesky factorization but produces the Cholesky factor simultaneously.

The truncated product and subtraction operations, \odot and \ominus , indicate the corresponding matrix operations which involve truncation to smaller ranks to maintain required accuracy. Here,

Algorithm 3.3a Block reordering

```
1: bodr( $\Sigma, \mathbf{a}, \mathbf{b}, m$ )
2:  $r = n/m$ 
3: for  $j = 1 : r$  do
4:    $\mathbf{p}[l] \approx \Phi_m(\mathbf{a}_l, \mathbf{b}_l; \Sigma_{l,l})$ 
5: end for
6: for  $j = 1 : r$  do
7:    $\tilde{j} = \operatorname{argmin}_l(\mathbf{p}[l]), l = j, \dots, r$ 
8:    $\mathbf{p}[j \rightleftharpoons \tilde{j}]$  and block-wise  $\Sigma[j \rightleftharpoons \tilde{j}, j \rightleftharpoons \tilde{j}], \mathbf{a}[j \rightleftharpoons \tilde{j}], \mathbf{b}[j \rightleftharpoons \tilde{j}]$ 
9: end for
```

Algorithm 3.3b Block reordering during Cholesky factorization

```
1: rbodr( $\Sigma, \mathbf{a}, \mathbf{b}, m$ )
2:  $r = n/m$ 
3: for  $j = 1 : r$  do
4:   for  $l = j : r$  do
5:      $\mathbf{p}[l] \approx \Phi_m(\mathbf{a}_l, \mathbf{b}_l; \Sigma_{l,l})$ 
6:   end for
7:    $\tilde{j} = \operatorname{argmin}_l(\mathbf{p}[l]), l = j, \dots, r$ 
8:   Block-wise  $\Sigma[j \rightleftharpoons \tilde{j}, j \rightleftharpoons \tilde{j}], \mathbf{a}[j \rightleftharpoons \tilde{j}], \mathbf{b}[j \rightleftharpoons \tilde{j}]$ 
9:    $\mathbf{y}_j \approx E_m[\mathbf{Y} | \mathbf{Y} \sim N_m(\mathbf{0}, \Sigma_{j,j}), \mathbf{Y} \in (\mathbf{a}_j, \mathbf{b}_j)]$ 
10:   $\Sigma_{j,j} = \text{Cholesky}(\Sigma_{j,j})$ 
11:  for  $i = j + 1 : r$  do
12:     $\Sigma_{i,j} = \Sigma_{i,j} \odot \Sigma_{j,j}^{-\top}$ 
13:     $\mathbf{a}_i = \mathbf{a}_i - \Sigma_{i,j} \odot \mathbf{y}_j, \mathbf{b}_i = \mathbf{b}_i - \Sigma_{i,j} \odot \mathbf{y}_j$ 
14:  end for
15:  for  $j_1 = j + 1 : r$  do
16:    for  $i_1 = j + 1 : r$  do
17:       $\Sigma_{i_1,j_1} = \Sigma_{i_1,j_1} \ominus \Sigma_{i_1,j} \odot \Sigma_{j_1,j}^{\top}$ 
18:    end for
19:  end for
20: end for
```

$\Sigma_{i_1,j} \odot \Sigma_{j_1,j}^{\top}$ and $\Sigma_{i,j} \odot \Sigma_{j,j}^{-\top}$ have complexities of $O(mk^2)$ and $O(m^2k)$ respectively, where m is the tile size and k is the local rank. The \ominus operation uses ACA truncated at an absolute tolerance to keep the result low-rank. For the studies in Section 4 and Section 5, we set the tolerance to 10^{-5} . Prior to the TLR Cholesky factorization, we construct the TLR covariance matrix with ACA given the covariance kernel, the underlying geometry and the indices of variables. Therefore, the total memory needed for computing MVN and MVT probabilities is $O(kn^2/m)$.

3.4 Preconditioned TLR QMC algorithms

Algorithm 3.4a and Algorithm 3.4b describe the TLR versions of the ‘mvn’ and ‘mvt’ algorithms. To distinguish them from the dense ‘mvn’ and ‘mvt’ algorithms, we expand the storage structure of \mathbf{C} , the TLR Cholesky factor, as the interface of the TLR algorithms. The definitions of \mathbf{B}_i , $\mathbf{U}_{i,j}$, and $\mathbf{V}_{i,j}$ are shown in Figure 1.

Similar to Algorithm 3.3b, we use subscripts to represent the size- m segment of \mathbf{a} , \mathbf{b} , \mathbf{y} ,

Algorithm 3.4a TLR QMC for MVN probabilities

```

1: tlrnmvn( $\mathbf{B}, \mathbf{U}, \mathbf{V}, \mathbf{a}, \mathbf{b}, \mathbf{w}$ )
2:  $\mathbf{y} \leftarrow \mathbf{0}$ , and  $P \leftarrow 1$ 
3: for  $i = 1 : r$  do
4:   if  $i > 1$  then
5:     for  $j = i : r$  do
6:        $\Delta = \mathbf{U}_{j,i-1}(\mathbf{V}_{j,i-1}^T \mathbf{y}_{i-1})$ 
7:        $\mathbf{a}_j = \mathbf{a}_j - \Delta$ ,  $\mathbf{b}_j = \mathbf{b}_j - \Delta$ 
8:     end for
9:   end if
10:   $(P', \mathbf{y}_i) \leftarrow \text{MVN}(\mathbf{B}_i, \mathbf{a}_i, \mathbf{b}_i, \mathbf{w}_i)$ 
11:   $P \leftarrow P \cdot P'$ 
12: end for
13: return  $P$ 

```

Algorithm 3.4b TLR QMC for MVT probabilities

```

1: tlrnmvt( $\mathbf{B}, \mathbf{U}, \mathbf{V}, \mathbf{a}, \mathbf{b}, \nu, w_0, \mathbf{w}$ )
2:  $\mathbf{a}' \leftarrow \frac{\chi_\nu^{-1}(w_0)}{\sqrt{\nu}} \mathbf{a}$ ,  $\mathbf{b}' \leftarrow \frac{\chi_\nu^{-1}(w_0)}{\sqrt{\nu}} \mathbf{b}$ 
3: return  $\text{TLRMVN}(\mathbf{B}, \mathbf{U}, \mathbf{V}, \mathbf{a}', \mathbf{b}', \mathbf{w})$ 

```

and \mathbf{w} . The two algorithms compute the integrand given one sample \mathbf{w} in the n -dimensional unit hypercube. In our implementation, the Richtmyer rule (Richtmyer, 1951), recommended by Genz and Bretz (2009), is employed for choosing \mathbf{w} . Here, ‘tlrmvn’ is called by ‘tlrmvt’, where the additional inputs, ν and w_0 , bear the same meaning as those in Algorithm 2.2b. The TLR structure reduces dense matrix-vector multiplication to low rank matrix-vector multiplication when factoring the correlation between blocks into the integration limits. The TLR structure reduces the complexity of matrix-vector multiplication, hence the cost per MC sample, at the step of block updating the integration limits (Lines 6 and 7 in Algorithm 3.4a). The TLR

QMC is a variant of the SOV algorithm from Genz (1992) that belongs to the same category as the hierarchical QMC (Genton et al., 2018). Algorithm 3.4a and Algorithm 3.4b can be either preconditioned by the block reordering or the iterative block reordering. We examine the performance of the TLR QMC algorithms in Section 4.

4 Numerical Simulations

Table 2 summarizes the performance of the dense (Genz, 1992) and the TLR QMC methods for computing MVN and MVT probabilities, measured on a workstation with 50 GB memory and 8 Xeon(R) E5-2670 CPUs. Methods are assessed over 20 simulated problems for each combination of problem dimension n and correlation strength β . The highest dimension in our experiment is 2^{16} . Considerations for higher dimensions include the truncation level required for the success of the TLR Cholesky factorization and the number of QMC samples needed to reach the desired accuracy. Here, $\beta = 0.3, 0.1, \text{ and } 0.03$ correspond to an effective range of 0.90, 0.30, and 0.09, the first of which is considered long given that the underlying geometry lies in the unit square. The tile size m for the TLR QMC methods is set as \sqrt{n} but other reasonable choices also suffice. The listed time covers only the integration part while the time for constructing the covariance matrix, the block reordering, and the Cholesky factorization is not included. The cost for Cholesky factorization is trivial compared with that for the integration while the cost for the non-iterative block reordering is minimal. The sample size is set at $N = 10^4$ for the methods without any preconditioner while at $N = 10^3$ for the four preconditioned methods to highlight the time efficiency of the preconditioned methods for reaching a similar accuracy.

Table 2 shows that the preconditioned methods achieve an even lower estimation error with one-tenth of the sample size compared with the ones without any preconditioner. The scalability of the TLR methods is better than the dense methods and the time saving already reaches two orders of magnitude in 16,384 dimensions. The iterative block reordering has a marginal improvement on the convergence rate over the non-iterative version. It is worth noting that the

block reorderings are more effective when heterogeneity is strong among the spatial variables. They would make no difference in the extreme scenario, where the correlation is constant and the integration limits are the same. The upper limits we choose for Table 2 are relatively big, whereas MVN and MVT problems with much smaller probabilities may appear in applications. In fact with 10^4 samples, the non-preconditioned methods already fail to provide a meaningful estimate

Table 2: Performance of the eight methods under strong, medium, and weak correlations. ‘mvn’ and ‘mvt’ are the dense QMC methods, ‘tlrmvn’ and ‘tlrmvt’ are the TLR QMC methods, ‘rtlrmvn’ and ‘rtlrmvt’ add the block reordering preconditioner to ‘tlrmvn’ and ‘tlrmvt’ while ‘rrtlrmvn’ and ‘rrtlrmvt’ use the iterative block reordering preconditioner. The covariance matrix, integration limits, and the degrees of freedom are generated the same way as in Table 1. The upper row is the average relative estimation error and the lower row is the average computation time over 20 replicates.

$\beta = 0.3$ (strong correlation)								
n	mvn	tlrmvn	rtlrmvn	rrtlrmvn	mvt	tlrmvt	rtlrmvt	rrtlrmvt
1024	0.5%	0.5%	0.4%	0.5%	0.6%	1.3%	1.3%	1.4%
	<i>2.1s</i>	<i>1.0s</i>	<i>0.1s</i>	<i>0.1s</i>	<i>2.2s</i>	<i>1.1s</i>	<i>0.1s</i>	<i>0.1s</i>
4096	1.0%	1.0%	0.9%	1.0%	1.1%	1.3%	1.2%	1.2%
	<i>44.8s</i>	<i>9.9s</i>	<i>0.9s</i>	<i>0.9s</i>	<i>44.7s</i>	<i>9.1s</i>	<i>0.8s</i>	<i>0.8s</i>
16384	2.4%	1.9%	1.9%	1.7%	2.1%	3.1%	2.4%	2.3%
	<i>1227.0s</i>	<i>60.1s</i>	<i>5.0s</i>	<i>5.0s</i>	<i>1214.9s</i>	<i>57.8s</i>	<i>4.8s</i>	<i>4.8s</i>
65536	NaN	5.7%	3.7%	3.2%	NaN	7.9%	5.9%	5.4%
	<i>NaN</i>	<i>308.6s</i>	<i>28.0s</i>	<i>28.8s</i>	<i>NaN</i>	<i>307.1s</i>	<i>27.5s</i>	<i>28.2s</i>
$\beta = 0.1$ (medium correlation)								
n	mvn	tlrmvn	rtlrmvn	rrtlrmvn	mvt	tlrmvt	rtlrmvt	rrtlrmvt
1024	0.5%	0.5%	0.3%	0.3%	0.5%	0.6%	0.6%	0.6%
	<i>2.0s</i>	<i>0.9s</i>	<i>0.1s</i>	<i>0.1s</i>	<i>1.9s</i>	<i>0.9s</i>	<i>0.1s</i>	<i>0.1s</i>
4096	1.3%	1.2%	1.1%	1.2%	1.3%	1.3%	1.1%	1.0%
	<i>40.2s</i>	<i>5.6s</i>	<i>0.4s</i>	<i>0.4s</i>	<i>40.8s</i>	<i>5.8s</i>	<i>0.5s</i>	<i>0.5s</i>
16384	4.1%	4.5%	3.9%	3.5%	3.6%	4.1%	3.7%	3.8%
	<i>1213.5s</i>	<i>44.1s</i>	<i>3.5s</i>	<i>3.4s</i>	<i>1204.3s</i>	<i>44.6s</i>	<i>3.5s</i>	<i>3.5s</i>
65536	NaN	29.2%	11.0%	10.4%	NaN	19.7%	10.6%	9.6%
	<i>NaN</i>	<i>302.9s</i>	<i>26.2s</i>	<i>26.4s</i>	<i>NaN</i>	<i>287.7s</i>	<i>24.3s</i>	<i>24.5s</i>
$\beta = 0.03$ (weak correlation)								
n	mvn	tlrmvn	rtlrmvn	rrtlrmvn	mvt	tlrmvt	rtlrmvt	rrtlrmvt
1024	0.1%	0.1%	0.1%	0.1%	0.2%	0.2%	0.3%	0.3%
	<i>2.0s</i>	<i>0.9s</i>	<i>0.1s</i>	<i>0.1s</i>	<i>2.1s</i>	<i>0.9s</i>	<i>0.1s</i>	<i>0.1s</i>
4096	0.7%	0.7%	0.4%	0.4%	0.6%	0.7%	0.6%	0.7%
	<i>39.6s</i>	<i>5.6s</i>	<i>0.4s</i>	<i>0.4s</i>	<i>39.8s</i>	<i>5.7s</i>	<i>0.4s</i>	<i>0.4s</i>
16384	3.7%	4.1%	2.7%	2.4%	3.8%	3.4%	1.9%	2.0%
	<i>1202.3s</i>	<i>37.3s</i>	<i>2.2s</i>	<i>2.2s</i>	<i>1197.7s</i>	<i>37.3s</i>	<i>2.2s</i>	<i>2.2s</i>
65536	NaN	87.7%	15.0%	14.0%	NaN	23.7%	13.1%	10.6%
	<i>NaN</i>	<i>219.7s</i>	<i>16.6s</i>	<i>16.6s</i>	<i>NaN</i>	<i>223.2s</i>	<i>16.7s</i>	<i>16.9s</i>

when $n = 65,536$ and $\beta = 0.03$. The convergence rate generally decreases for small integration limits, where importance sampling techniques, for example, Botev (2017), become necessary in reducing the sample size. However, in this paper, we do not resort to importance sampling but suggest that the preconditioned methods provide a decent estimate for the log-probability in relatively high dimensions.

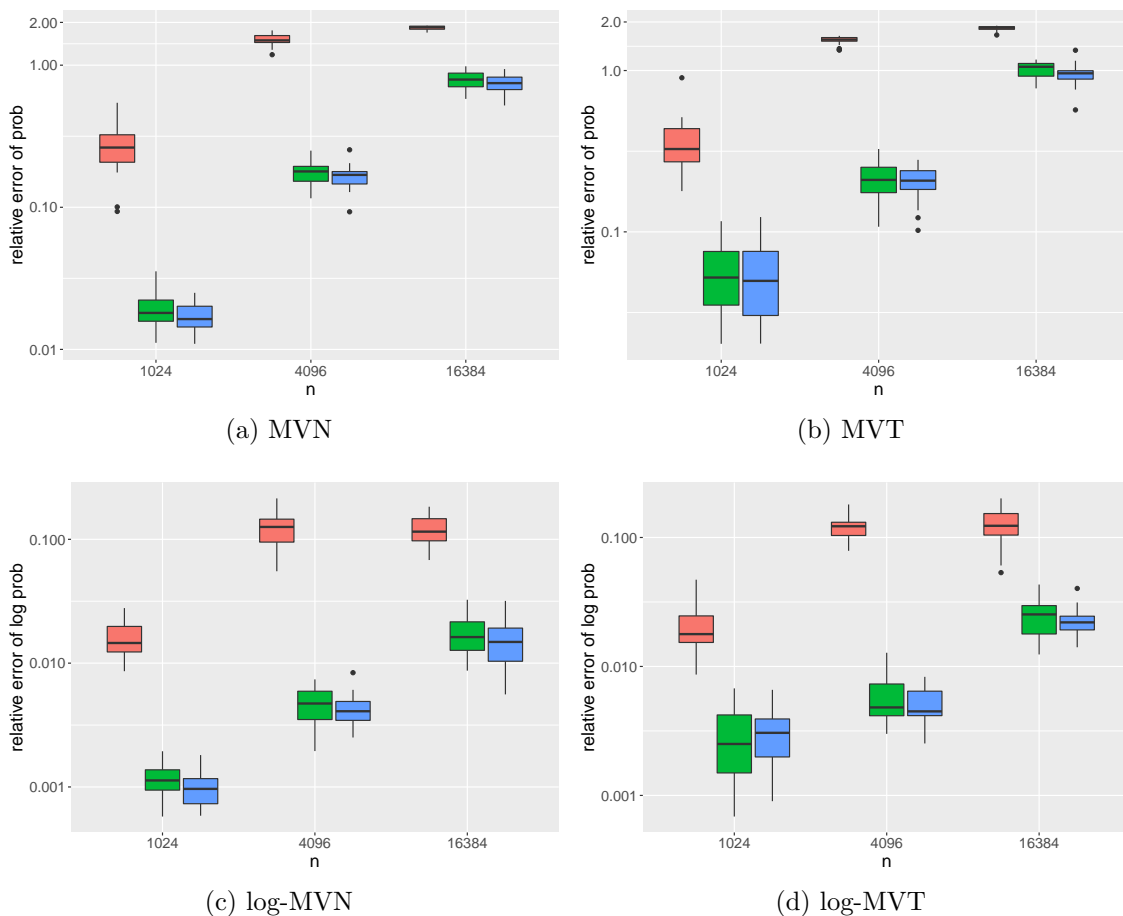


Figure 4: The relative error for probabilities and log-probabilities. For each n , the three boxplots, from left to right, correspond to the TLR method, the TLR with the block reordering method, and the TLR with the iterative block reordering method. The relative error for log-probabilities is based on 10 estimations of the same replicate. Each boxplot consists of 20 replicates. The covariance matrix, degrees of freedom, and lower integration limits are the same as Table 1 ($\beta = 0.1$) while the upper limits are generated from $N(4.0, 1.5^2)$.

Figure 4 compares the relative error for the probabilities and the log-probabilities, where the simulated problems have smaller integration limits generated from $N(4.0, 1.5^2)$. The ‘mvt’ and ‘mvt’ methods are not included because they share the same error level as the ‘tlrmvt’

and ‘tlrmvt’ methods and the sample size N for all listed methods is 10^4 . The error for the log-probability cannot be directly estimated, for which the same problem is estimated 10 times to provide replicates of the log-probabilities. In terms of the relative error for probabilities, all methods fail to provide a meaningful estimate when $n = 16,384$. However, the relative error for the log-probability is significantly smaller, which indicates that the methods are relatively reliable if we use the logarithm of the estimates and that the distribution of the estimates has significant skewness. Consistent with Table 2, the iterative block reordering outperforms the non-iterative version while both have a considerably higher convergence rate than the non-preconditioned versions. We show that the log-probability estimated from the preconditioned methods is sufficient for the maximum likelihood procedure in Section 5.

5 Application to Stochastic Generators

5.1 A skew-normal stochastic generator

Stochastic generators model the space-time dependence of the data in the framework of statistics and aim to reproduce the physical process that is usually emulated through a system of partial differential equations. The emulation of the system requires tens of variables and a very fine grid in the spatio-temporal domain, which is extremely time-and-storage demanding (Castruccio and Genton, 2016). For example, the Community Earth System Model (CESM) Large ENsemble project (LENS) required ten million CPU hours and more than four hundred terabytes of storage to emulate one initial condition (Jeong et al., 2018). Castruccio and Genton (2016) found statistical models could form efficient surrogates for reproducing the physical processes in climate science and concluded that extra model flexibilities would facilitate the modeling on a finer scale; see Castruccio and Genton (2018) for a recent account.

The MVN and MVT methods developed in this paper allow to consider more complexity in the construction of stochastic generators. A significant improvement in flexibility is to introduce

skewness since the majority of the statistical models used nowadays are Gaussian-based, i.e. they rely on a symmetric distribution. Generally speaking, there are three ways of introducing skewness to an elliptical distribution, all of which involve the cdf of the distribution. The first is through reformulation, which multiplies the elliptical probability density function (pdf) by its cdf. The second method introduces skewness via selection. Assuming $(\mathbf{X}^\top, \mathbf{Y}^\top)^\top$ have a joint multivariate elliptical distribution, $\mathbf{X}|\mathbf{Y} > \boldsymbol{\mu}$, where $\boldsymbol{\mu}$ is an n -dimensional vector, has a skew-elliptical distribution. Arellano-Valle and Genton (2010) studied a general class of skewed reformulations and introduced its link to the selection representation. The third method is defined by the stochastic representation, specifically, $\mathbf{Z} = \mathbf{X} + |\mathbf{Y}|$, where \mathbf{X} and \mathbf{Y} are two independent elliptical random vectors. Zhang and El-Shaarawi (2010) studied the skew-normal random field based on this construction assuming a general correlation structure for \mathbf{Y} , because of which a direct maximum likelihood estimation is almost impossible. Instead, \mathbf{Y} was taken as a latent random variable and the EM algorithm was applied. In the M-step, the conditional expectations of \mathbf{X} were computed through the Markov chain Monte Carlo method. Thus, the cost for maximizing the likelihood is expectedly high.

The three methods have equivalent forms in the one-dimensional case but extend differently into higher dimensions. The first method is flexible but provides little information on the underlying stochastic process. The second method has a clear underlying model and its pdf is usually more tractable than that from the third method but the choice for \mathbf{Y} is usually not obvious, especially when \mathbf{X} is in high dimensions. In the third method, the parameterization is usually more intuitive and the model can be also applied in spatial statistics as a random field. However, the pdf is a summation of a number of terms exponentially growing with the number of locations n , which renders the model difficult to scale. Weighing an intuitive stochastic representation against the pdf complexity, we modify the third construction method based on the \mathcal{C} random vector properties introduced in Arellano-Valle et al. (2002). A \mathcal{C} random vector can be written as the Hadamard product of two independent random vectors, representing the sign and the magni-

tude, respectively. When \mathbf{Y} is a \mathcal{C} random vector and \mathbf{X} is independent from \mathbf{Y} , $G(\mathbf{X}, \mathbf{Y})|\mathbf{Y} > \mathbf{0}$ has the same distribution as $G(\mathbf{X}, |\mathbf{Y}|)$ for any function $G(\cdot)$ (Arellano-Valle et al., 2002). Similar to these authors, our model assumes a stochastic representation where the matrix-vector multiplication that models the dependence structure among the skewness components follows the absolute value operation:

$$\mathbf{Z}^* = \xi \mathbf{1}_n + \mathbf{A}\mathbf{X} + \mathbf{B}|\mathbf{Y}|, \quad (5)$$

where $\xi \in \mathbb{R}$ is the location parameter, $\{X_i|i = 1, \dots, n\} \cup \{Y_i|i = 1, \dots, n\}$ are independent and identically distributed standard normal random variables. Hence, $\mathbf{A}\mathbf{X} + \mathbf{B}|\mathbf{Y}|$ has the same distribution as $\mathbf{A}\mathbf{X} + \mathbf{B}\mathbf{Y}|\mathbf{Y} > \mathbf{0}$ since we can choose $G(\mathbf{X}, \mathbf{Y})$ to be $\mathbf{A}\mathbf{X} + \mathbf{B}\mathbf{Y}$. The pdf of \mathbf{Z}^* avoids the 2^n -term summation, which was the hinge in Zhang and El-Shaarawi (2010), making the pdf computation more scalable.

The marginal representation shown in Equation (5) is difficult to extend to the multivariate skewed- t version because the sufficient condition for the equivalence between the conditional representation and the marginal representation is that \mathbf{X} and \mathbf{Y} are independent (Arellano-Valle et al., 2002). However, the sum of independent Student- t random variables does not necessarily lead to another Student- t random variable. Another issue with this representation is the difficulty to generalize as a random field. When \mathbf{A} is a Cholesky factor, $\mathbf{A}\mathbf{X}$ coincides with the classical Gaussian random field but it is not obvious that $\mathbf{B}|\mathbf{Y}|$ can be derived from any well-defined random field. However, for stochastic generators, the model is usually simulated on a fixed spatial domain without the need for prediction at unknown locations and therefore, Equation (5) may serve as the surrogate model for a physical system. In general, this stochastic representation has better-rounded properties due to its advantage in estimation, simulation, and flexibility. Specifically,

- the pdf avoids the summation of 2^n terms as in the model $\mathbf{A}\mathbf{X} + |\mathbf{B}\mathbf{Y}|$, which makes the pdf estimable;

- the marginal representation in Equation (5) allows for more efficient simulation compared with conditional representations;
- the correlation structure between the skewness components $\mathbf{B}|\mathbf{Y}|$ has full flexibility controlled by \mathbf{B} , which can adapt to different datasets for model fitting.

Considering the reasons above, we simulate \mathbf{Z}^* based on the skew-normal distribution without tapping into any skewed Student- t counterpart for the simulation study and use the same model as a stochastic generator for the Saudi wind speed dataset that has more than 18,000 spatial locations.

5.2 Estimation with simulated data

We construct \mathbf{A} and \mathbf{B} before simulating \mathbf{Z}^* , where \mathbf{A} controls the correlation strength of the symmetric component while \mathbf{B} adjusts the level of skewness and the correlation between the skewness component. To have a parsimonious model, \mathbf{A} is assumed to be the lower Cholesky factor of a covariance matrix constructed from the 2D exponential kernel, $\sigma_1^2 \exp(-\|\mathbf{h}\|/\beta_1)$, $\beta_1 > 0$, and \mathbf{B} takes the form of a covariance matrix from the kernel, $\sigma_2^2 \exp(-\|\mathbf{h}\|/\beta_2)$, $\beta_2 > 0$, where \mathbf{h} is the vector connecting the two spatial variables' locations. We choose the form of a covariance matrix instead of a Cholesky factor for \mathbf{B} out of two reasons. Numerically, the row sum of a Cholesky factor usually increases with the row index, which produces a large difference between the sum of the first row and that of the last row when the dimension is high. This would cause the coefficients of \mathbf{Z}^* to have a varying order of magnitude. Secondly, due to the first reason, the likelihood would depend on the ordering of the random variables in \mathbf{Z}^* . When \mathbf{B} is a covariance matrix, the row sums usually have similar magnitudes and the likelihood function becomes independent from the ordering scheme. The pdf of \mathbf{Z}^* can be derived based on the results in Arellano-Valle et al. (2002) to be:

$$2^n \phi_n(\mathbf{z} - \xi \mathbf{1}_n, \mathbf{A}\mathbf{A}^\top + \mathbf{B}\mathbf{B}^\top) \Phi_n\{-\infty, (\mathbf{I}_n + \mathbf{C}^\top \mathbf{C})^{-1} \mathbf{C}^\top \mathbf{A}^{-1}(\mathbf{z} - \xi \mathbf{1}_n); (\mathbf{I}_n + \mathbf{C}^\top \mathbf{C})^{-1}\}, \quad (6)$$

where $\mathbf{C} = \mathbf{A}^{-1}\mathbf{B}$. Assuming a dense representation, the matrix operations have $O(n^3)$ complexity. However, the TLR representation can closely approximate $\mathbf{A}\mathbf{A}^\top$ and \mathbf{B} due to the 2D exponential covariance model. The subsequent Cholesky factorization, matrix multiplication, and matrix inversion can be performed at adequate accuracy and the complexity can be reduced by one order of magnitude. For each $n = 4^r, r = 4, 5, 6, 7$, we generate the geometry in the

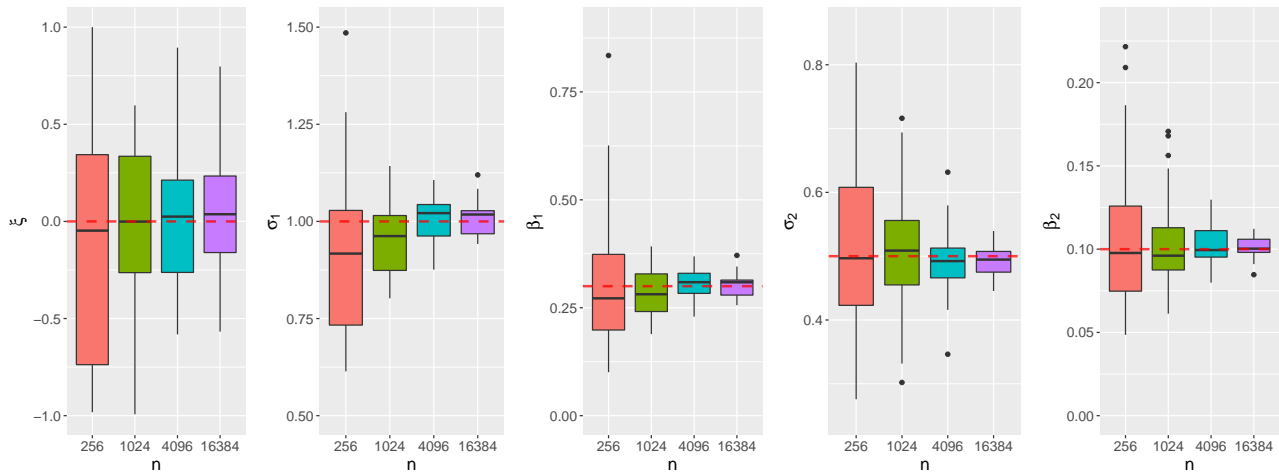


Figure 5: Boxplots of 30 estimation results. Each estimation is based on one realization of the n -dimensional skew-normal model. The red dashed line marks the true value used for generating random vectors from the skew-normal model.

$[0, 2^{r-4}] \times [0, 2^{r-4}]$ square, mimicking an expanding domain. The spatial locations are on a perturbed grid, where the grid's length unit is $1/15$ and the perturbation is uniformly distributed within $(-0.4/15, 0.4/15)^2$. Here, \mathbf{A} and \mathbf{B} are constructed based on the covariance kernel and the simulated geometry. The likelihood function is the pdf of \mathbf{Z}^* shown in Equation (6) and the optimization seeks to find the parameter values that maximize the likelihood when \mathbf{z} is fixed. In each run, the geometry is regenerated and only dense representations are used for the simulation of \mathbf{Z}^* to avoid bias. The optimization employs the Controlled Random Search (CRS) with local mutation algorithm (Kaelo and Ali, 2006) from the NLOpt library (Johnson, 2014). The true values for $(\xi, \sigma_1, \beta_1, \sigma_2, \beta_2)$ are shown in Figure 5 and their searching ranges are $(-1.0, 1.0)$, $(0.1, 2.0)$, $(0.01, 0.9)$, $(0.0, 1.0)$, and $(0.01, 0.3)$, respectively.

The initial values for the four parameters are set equal to the lower limits of their searching

ranges and the stopping condition is a convergence level of 10^{-3} . The boxplots for the four chosen dimensions each consisting of 30 estimations are shown in Figure 5. Overall, the estimation improves as the dataset dimension n increases. The outliers may indicate that there is a local maximum, where σ_1 and β_1 are large and σ_2 is small, on a similar magnitude level with the global maximum. In this case, the estimation result is closer to a Gaussian random field.

In the application study, we found that the likelihood was extremely small when the dimension n was high because the order of magnitude cumulated through the multiplication of one-dimensional probabilities as shown in Equation (2), exceeding the lower boundary of double-precision numbers. We extracted the exponent after each multiplication step described on Line 9 of Algorithm 2.1a. This mechanism allows for a minimum value of 2^{MIN_INT} , where MIN_INT is the minimum integer allowed.

5.3 Estimation with wind data from Saudi Arabia

The dataset we use for modeling is the daily wind speed over a region in the Kingdom of Saudi Arabia on August 5th, 2013, produced by the WRF model (Yip, 2018), which numerically predicts the weather system based on partial differential equations on the mesoscale and features strong computation capacity to serve meteorological applications (Skamarock et al., 2008). The dataset has an underlying geometry with 155 longitudinal and 122 latitudinal bands. Specifically, the longitude increases from 40.034 to 46.960 and the latitude increases from 16.537 to 21.979, both with an incremental size of 0.045. Before fitting the skew-normal model, we subtract the wind speed at each location with its mean over a six-year window (six replicates in total) to increase the homogeneity across the locations. The vectorized demeaned wind speed data is used as the input dataset, \mathbf{Z}^* , for the maximum likelihood estimation. The dataset has a skewness of -0.45 and is likely to benefit from the skewness flexibility introduced by the model in Equation (5). It is worth noting that $\mathbf{B}|\mathbf{Y}|$ has a negative skewness under our parameterization for \mathbf{B} although all its coefficients are non-negative.

The likelihood function is described in Equation (6), where the parameterization of \mathbf{A} and \mathbf{B} also remains unchanged. The optimization involves five parameters, namely ξ , σ_1 , β_1 , σ_2 , and β_2 , whose searching ranges, initial values, and optimized values are listed in Table 3. Since the likelihood requires the inverse of \mathbf{A} as shown in Equation (6), we set the lower limit of σ_1 to 0.1 to avoid the singularity. The correlation-strength parameters β_1 and β_2 can theoretically be close to zero but setting a lower limit above zero can avoid boundary issues. The convergence level is set at 10^{-3} and the optimization produces the results shown in Table 3, which has a (negative) log-likelihood of 11,508. We compare the optimized skew-normal model with the optimized classical Gaussian random field, which is also a simplified version of Equation (5), where σ_2 is fixed at zero: $\mathbf{Z}^* = \xi \mathbf{1}_n + \mathbf{A}\mathbf{X}$. The estimation of the Gaussian random field thus involves three parameters, (σ_1, β_1, ξ) , for which the optimization setups are the same as those for the skew-normal model. The estimated parameter values are also summarized in Table 3, which has a (negative) log-likelihood of 10,797. The functional boxplots (Sun and Genton, 2011) of the empirical semivariogram based on 100 simulations of the fitted skew-normal model and the Gaussian random field are shown in Figure 6. The skew-normal model has significantly smaller band width than the Gaussian random field in the semivariogram plot, although both cover the semivariogram of the original data. The BIC values of the two models and the quantile intervals of the empirical moments based on the same 100 simulations are illustrated in Table 4. The BIC values strongly indicate that the skew-normal model is a better fit than the Gaussian random field. This can be also seen from the variance quantile intervals and the functional boxplots of

Table 3: Parameter specifications and estimations based on the skew-normal (SN) model and the Gaussian random field (GRF)

	ξ	σ_1	β_1	σ_2	β_2
Range	$(-2, 2)$	$(0.1, 2.0)$	$(0.1, 5.0)$	$(0.0, 2.0)$	$(0.01, 1.0)$
Initial Value	0.000	1.000	0.100	1.000	0.010
SN	-1.211	1.028	4.279	0.419	0.065
GRF	0.338	1.301	4.526	N.A.	N.A.

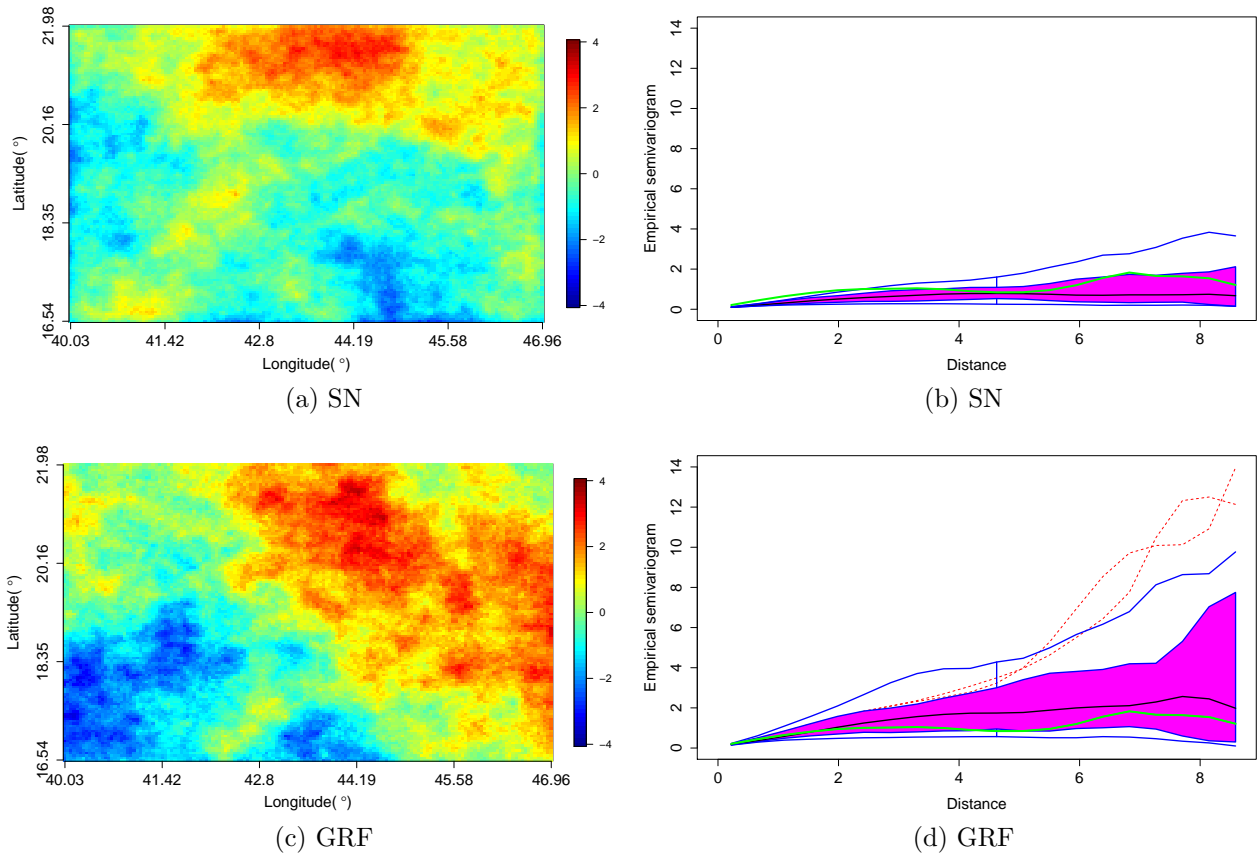


Figure 6: The heatmap based on one simulation and the functional boxplot of the empirical semivariogram based on 100 simulations. Top to bottom are the fitted skew-normal model and the Gaussian random field. The green curve denotes the empirical semivariogram based on the wind speed data. The distance is computed as the Euclidean distance in the longitudinal and latitudinal coordinate system.

the empirical semivariogram, where the former has smaller variance and its semivariogram is more aligned with that of the Saudi wind data. The empirical moments ignore the connection between the spatial locations, thus may not be a comprehensive measure for the fitting quality.

Table 4: Empirical moments and BIC comparison. SN denotes the skew-normal model and GRF denotes the Gaussian random field. The intervals represent the 5% to 95% quantile intervals based on 100 simulations.

	Mean	Variance	Skewness	Kurtosis	BIC
Wind data	0.042	0.932	-0.445	2.873	N.A.
SN	(-1.079, 1.360)	(0.308, 1.054)	(-0.644, 0.449)	(2.274, 3.595)	-22986
GRF	(-1.644, 1.911)	(0.612, 2.594)	(-0.717, 0.489)	(2.116, 3.705)	-21565

Except for the one for the variance, the two models are not significantly different in terms of the other three quantile intervals.

6 Conclusion

In this paper, we first summarized the SOV methods from Genz (1992) and Genz and Bretz (1999) for MVN and MVT probabilities. Two definitions of the MVT probability were compared and one was shown to have better numerical properties than the other. Next, we demonstrated that the hierarchical representation used in Genton et al. (2018) is not aligned with variable reordering, specifically, with the block reordering from Cao et al. (2019), while the TLR (Akbulak et al., 2017) representation combined with the block reordering benefits from both a higher convergence rate and lower costs per MC sample. Additionally, an iterative version of the block reordering was proposed based on the original version in Cao et al. (2019) that further improves the convergence rate and produces the TLR Cholesky factor simultaneously. A third contribution of this paper is the finding that although the relative error based on the MC simulation may render the estimation ‘meaningless’, the estimates of the log-probabilities are still sufficiently accurate for many applications. This makes several SOV variants still applicable in relatively high dimensions without resorting to the expensive importance sampling technique (Botev, 2017). However, importance sampling becomes necessary for demanding applications, for example, the numerical computation of derivatives. Finally, we used both simulated and physical datasets in tens of thousands of dimensions to illustrate the capability of our methods in terms of model estimation, where the TLR variant of the SOV method improved the time efficiency by two orders of magnitude compared with the original SOV method in Genz (1992).

Acknowledgements

The authors thank Prof. Georgiy Stenchikov at KAUST for providing the WRF data.

References

- Akbulduk, K., Ltaief, H., Mikhalev, A., and Keyes, D. (2017), “Tile low rank cholesky factorization for climate/weather modeling applications on manycore architectures,” in *International Supercomputing Conference*, Springer, pp. 22–40.
- Arellano-Valle, R., del Pino, G., and San Martín, E. (2002), “Definition and probabilistic properties of skew-distributions,” *Statistics & Probability Letters*, 58, 111–121.
- Arellano-Valle, R. B., Branco, M. D., and Genton, M. G. (2006), “A unified view on skewed distributions arising from selections,” *Canadian Journal of Statistics*, 34, 581–601.
- Arellano-Valle, R. B. and Genton, M. G. (2010), “Multivariate unified skew-elliptical distributions,” *Chilean Journal of Statistics*, 1, 17–33.
- Azzalini, A. and Capitanio, A. (2014), *The Skew-Normal and Related Families*, Cambridge University Press.
- Bebendorf, M. (2011), “Adaptive cross approximation of multivariate functions,” *Constructive Approximation*, 34, 149–179.
- Bolin, D. and Lindgren, F. (2015), “Excursion and contour uncertainty regions for latent Gaussian models,” *Journal of the Royal Statistical Society: Series B (Statistical Methodology)*, 77, 85–106.
- Botev, Z. I. (2017), “The normal law under linear restrictions: simulation and estimation via minimax tilting,” *Journal of the Royal Statistical Society: Series B (Statistical Methodology)*, 79, 125–148.
- Boukaram, W., Turkiyyah, G., and Keyes, D. (2019), “Hierarchical matrix operations on GPUs: Matrix-vector multiplication and compression,” *ACM Transactions on Mathematical Software*, 45, 3:1–3:28.
- Cao, J., Genton, M. G., Keyes, D. E., and Turkiyyah, G. M. (2019), “Hierarchical-block conditioning approximations for high-dimensional multivariate normal probabilities,” *Statistics and Computing*, 29, 585–598.
- Castruccio, S. and Genton, M. G. (2016), “Compressing an ensemble with statistical models: An algorithm for global 3D spatio-temporal temperature,” *Technometrics*, 58, 319–328.
- (2018), “Principles for statistical inference on big spatio-temporal data from climate models,” *Statistics & Probability Letters*, 136, 92–96.

- Durante, D. (2019), “Conjugate Bayes for probit regression via unified skew-normal distributions,” *Biometrika*, 106, 765–779.
- Genton, M. G. (2004), *Skew-elliptical Distributions and Their Applications: A Journey Beyond Normality*, CRC Press.
- Genton, M. G., Keyes, D. E., and Turkiyyah, G. (2018), “Hierarchical decompositions for the computation of high-dimensional multivariate normal probabilities,” *Journal of Computational and Graphical Statistics*, 27, 268–277.
- Genz, A. (1992), “Numerical computation of multivariate normal probabilities,” *Journal of Computational and Graphical Statistics*, 1, 141–149.
- Genz, A. and Bretz, F. (1999), “Numerical computation of multivariate t-probabilities with application to power calculation of multiple contrasts,” *Journal of Statistical Computation and Simulation*, 63, 103–117.
- (2002), “Comparison of methods for the computation of multivariate t probabilities,” *Journal of Computational and Graphical Statistics*, 11, 950–971.
- (2009), *Computation of Multivariate Normal and t Probabilities*, vol. 195, Springer Science & Business Media.
- Hackbusch, W. (2015), *Hierarchical Matrices: Algorithms and Analysis*, vol. 49, Springer.
- Jeong, J., Castruccio, S., Crippa, P., Genton, M. G., et al. (2018), “Reducing storage of global wind ensembles with stochastic generators,” *The Annals of Applied Statistics*, 12, 490–509.
- Johnson, S. G. (2014), “The NLopt nonlinear-optimization package,” <http://github.com/stevengj/nlopt>.
- Kaelo, P. and Ali, M. (2006), “Some variants of the controlled random search algorithm for global optimization,” *Journal of Optimization Theory and Applications*, 130, 253–264.
- Richtmyer, R. D. (1951), “The evaluation of definite integrals, and a quasi-Monte-Carlo method based on the properties of algebraic numbers,” Tech. rep., Los Alamos Scientific Lab.
- Samet, H. (1990), *The Design and Analysis of Spatial Data Structures*, vol. 85, Addison-Wesley Reading, MA.
- Schervish, M. J. (1984), “Algorithm AS 195: Multivariate normal probabilities with error bound,” *Journal of the Royal Statistical Society. Series C (Applied Statistics)*, 33, 81–94.

- Skamarock, W. C., Klemp, J. B., Dudhia, J., Gill, D. O., Barker, D. M., Duda, M. G., Huang, X.-Y., Wang, W., and Powers, J. G. (2008), *A Description of the Advanced Research WRF Version 3*, vol. 113, NCAR.
- Sun, Y. and Genton, M. G. (2011), “Functional boxplots,” *Journal of Computational and Graphical Statistics*, 20, 316–334.
- Trinh, G. and Genz, A. (2015), “Bivariate conditioning approximations for multivariate normal probabilities,” *Statistics and Computing*, 25, 989–996.
- Yip, C. M. A. (2018), “Statistical characteristics and mapping of near-surface and elevated wind resources in the Middle East,” Ph.D. thesis, King Abdullah University of Science and Technology.
- Zhang, H. and El-Shaarawi, A. (2010), “On spatial skew-Gaussian processes and applications,” *Environmetrics*, 21, 33–47.